



CHORUS

This is the accepted manuscript made available via CHORUS. The article has been published as:

## Spin Structure in an Interfacially Coupled Epitaxial Ferromagnetic Oxide Heterostructure

X. Ke, L. J. Belenky, V. Lauter, H. Ambaye, C. W. Bark, C. B. Eom, and M. S. Rzchowski

Phys. Rev. Lett. **110**, 237201 — Published 4 June 2013

DOI: [10.1103/PhysRevLett.110.237201](https://doi.org/10.1103/PhysRevLett.110.237201)

# Spin structure in an interfacially-coupled epitaxial ferromagnetic oxide heterostructure

X. Ke<sup>1,2,\*#</sup>, L. J. Belenky<sup>3</sup>, V. Lauter<sup>\*1</sup>, H. Ambaye<sup>1</sup>, C. W. Bark<sup>3</sup>, C. B. Eom<sup>3</sup>, and M. S. Rzchowski<sup>4</sup>

<sup>1</sup>*Neutron Sciences Directorate, Oak Ridge National Laboratory, Oak Ridge, TN 37831, USA*

<sup>2</sup>*Department of Physics and Astronomy, Michigan State University, East Lansing, MI 48824, USA*

<sup>3</sup>*Department of Materials Science and Engineering, University of Wisconsin-Madison, Madison, WI 53706, USA*

<sup>4</sup>*Department of Physics, University of Wisconsin-Madison, Madison, WI 53706, USA*

We report the spin structure of an exchange-biased ferromagnetic oxide heterostructure,  $\text{La}_{0.67}\text{Sr}_{0.33}\text{MnO}_3$  /  $\text{SrRuO}_3$ , through magnetization and polarized neutron reflectometry measurements. We reveal that the magnetization reversal process of the  $\text{La}_{0.67}\text{Sr}_{0.33}\text{MnO}_3$  biased layer critically depends on the frozen-in spin structure of the  $\text{SrRuO}_3$  biasing layer during the cooling process. Furthermore, we observe unexpected double-shifted hysteresis loops of the biased layer that originates from the formation of lateral  $180^\circ$  magnetic domains within the biasing layer, a new mechanism not found in conventional exchange-bias systems.

---

\* Authors contributed equally

# Corresponding author: ke@pa.msu.edu

Oxide heterostructures show novel properties arising from reconstruction at the interface [1], including lattice reconstruction, electronic reconstruction, and orbital reconstruction. These emergent interfacial phenomena have attracted intense attention in the past few years [2]. For instance, an exchange-bias phenomenon (the hysteresis loop off-centers from the origin along the field axis) has been observed in ferromagnetic oxide heterostructures [3,4].

In exchange-bias systems a magnetization loop shift of the (magnetically soft) ‘biased’ layer depends on the detailed spin configurations of the (magnetically hard) ‘biasing’ layer (which can be antiferromagnetic [5], ferrimagnetic [6], or ferromagnetic [3,4,7]). This spin configuration is set as the bilayer system is cooled through magnetic transition temperature of the biasing layer and depends on the external magnetic ‘cooling field’ (CF). The resulting spin configuration of the biasing layer is to first order ‘frozen’ at low temperature when the magnetic anisotropy becomes large, although the reversal of the biased layer during a magnetization loop can dynamically perturb the spin structure of the biasing layer by winding spiral spin configurations or partial domain walls parallel to the layer interface [8,9].

In most exchange-bias systems the interfacial exchange interaction is ferromagnetic, leading to an exchange field that is always opposite in sign to CF (negative exchange bias) [5]. In contrast, positive exchange-bias (loop shift along the CF direction) has been observed in a few systems, including Fe/FeF<sub>2</sub> [10], Gd<sub>40</sub>Fe<sub>60</sub>/Tb<sub>12</sub>Fe<sub>88</sub> [11], and La<sub>0.67</sub>Sr<sub>0.33</sub>MnO<sub>3</sub>/SrRuO<sub>3</sub> [3,4], where the biasing layers FeFe<sub>2</sub>, Tb<sub>12</sub>Fe<sub>88</sub>, and SrRuO<sub>3</sub> are antiferromagnet, ferrimagnet and ferromagnet, respectively, indicating an antiferromagnetic interfacial exchange coupling. In the former two cases, the sign of the exchange field changes from positive to negative with decreasing CF, which has been attributed to the formation of magnetic domain walls *parallel* to the bilayer interface induced in the biasing layer by field cooling [11].

Although the antiferromagnetic interfacial coupling has been established in the  $\text{La}_{0.67}\text{Sr}_{0.33}\text{MnO}_3$  (LSMO) /  $\text{SrRuO}_3$  (SRO) bilayers [3] and superlattices [4], the key issues regarding the spin structure of SRO biasing layer formed in the cooling process and its crucial effect on the biased LSMO magnetization reversal have remained elusive. In this paper, combining polarized neutron reflectometry (PNR) and bulk magnetization measurements, we have determined the frozen-in spin structure of SRO layer that depends on the competition between Zeeman interaction, interfacial antiferromagnetic interaction, and its uniaxial magnetic anisotropy. Furthermore, we have revealed unexpected double-shifted hysteresis loops of the LSMO biased layer, and attributed this feature to the formation of lateral  $180^\circ$  magnetic domains with *perpendicular* domain walls within the SRO biasing layer, which is a new mechanism not reported in conventional exchange-bias systems. This study sets an example of intriguing interfacial phenomena and illustrates the importance of interfacial coupling in complex oxide heterostructures.

The epitaxial bilayer heterostructures were grown on  $0.2^\circ$ -miscut and  $\text{TiO}_2$ -terminated (001)  $\text{SrTiO}_3$  substrates by pulsed laser deposition (PLD) with atomic layer control [3]. LSMO ( $\sim 13$  nm) was first grown at  $800^\circ\text{C}$  on substrates. SRO ( $\sim 24$  nm) was then grown at  $600^\circ\text{C}$  on top of the LSMO. This resulted in strained epitaxial LSMO and SRO layers as evidenced by the x-ray reciprocal space map about the (103) reciprocal lattice point (Fig.1). *Ex-situ* scanning tunneling microscopy (STM) measurement showed a terrace morphology of the topmost surface, with unit cell step heights and terrace widths consistent with the  $0.2^\circ$  miscut of the  $\text{SrTiO}_3$  substrate along the [100] direction (inset of Fig. 1). Magnetic properties of a sample with a size of  $\sim 0.21\text{ cm}^2$  were studied by a Quantum Design superconducting quantum interference device

(SQUID) magnetometer and by PNR on the time-of-flight Magnetism Reflectometer at Spallation Neutron Source in Oak Ridge National Laboratory.

The temperature dependence of magnetic moment of the bilayer (Fig. 2(a)) was measured while warming in a 1000 Oe field and shows a peculiar behavior after field-cooling the sample from 200 K to 10 K in various CFs applied along the substrate miscut direction (i.e, the SRO easy axis direction [12]). Before each cooling, a 2000 Oe field was applied at 200 K to saturate the LSMO layer ( $H_c$  of LSMO  $\sim$  30 Oe). Two magnetic transitions are clearly seen at  $T \sim$  340 K and 150 K for LSMO and SRO layers respectively. The intriguing features emerge when the SRO layer becomes ferromagnetic. In a 1000 Oe CF, the magnetic moment of the sample monotonically increases with decreasing temperature down to 5 K, indicating the parallel moment alignment of SRO and LSMO layers. In contrast, with a smaller CF, 100 Oe, the magnetic moment decreases sharply below 125 K before saturating at lower temperatures with a total moment smaller than that of an LSMO single layer (represented by the dash-dotted curve). This indicates that the net magnetic moment of SRO and LSMO layers have aligned *antiparallel* to each other, suggesting an *antiferromagnetic* interfacial coupling between these two components. First principles calculations have shown that such an antiferromagnetic coupling originates from the hybridization of interfacial O 2p with 3d state of Mn atoms and 4d state of Ru atoms [13,4]. Interestingly, with an intermediate CF, the net contribution of SRO magnetic moment increases, although being smaller than the full saturated moment of SRO layer, as depicted by the red curve shown in Fig. 2(a) for 500 Oe CF.

Magnetic hysteresis loops describing the LSMO layer magnetization reversal were obtained at 10 K with the magnetic field swept within  $\pm$  1500 Oe, as shown in Fig. 2(b), after field-cooling the sample from 200 K. It is noteworthy that the SRO layer has a much stronger

magnetic anisotropy [12], with coercivity larger than 1 Tesla at 10 K. It is thus expected that the SRO moment remains unchanged during the  $\pm 1500$  Oe field sweep. The hysteresis loop is rigidly shifted along the positive field axis for 1000 Oe CF, indicating that the LSMO layer has *positive* exchange-bias. This is consistent with the scenario of energy-preferable interfacial antiferromagnetic coupling. In addition, the hysteresis loop is shifted along the positive magnetization axis due to the fixed moment of the SRO biasing layer pinned along the field axis. While for 100 Oe CF, the hysteresis loop is shifted along the negative direction of both field and magnetization axes, namely, the LSMO layer has *negative* exchange-bias. Intriguingly, with an intermediate CF there appears a double-loop hysteresis behavior and a smaller shift along the magnetization axis. We argue that this arises from magnetic domain structures formed within the SRO layer: domain walls *perpendicular* to the bilayer interface separating lateral magnetic domains of two opposite SRO magnetization orientations, each of which biased the LSMO regions directly below those domains to opposite directions.

The net magnetization of SRO layer at 10 K can be extracted from both the hysteresis loops as  $M_{MH}^{SRO} = (M^+ + M^-)/2$ , where  $M^+$  and  $M^-$  represent the total magnetic moment at  $\pm 1000$  Oe respectively, and from the  $M(T)$  curves shown in Fig. 2(a),  $M_{MT}^{SRO}$ . The comparable values of  $M_{MH}^{SRO}$  and  $M_{MT}^{SRO}$  and their linear relationship (inset of Fig. 2(c)) confirm the frozen-in spin structure of SRO layer after the cooling process, consistent with strong magnetic anisotropy of SRO. Fig. 2(c) shows the CF dependence of the extracted SRO moment, which changes sign from negative to positive with increasing CF, representing the increasing proportion of SRO domains with a spin configuration parallel to the LSMO layer. In contrast to other bilayer systems [10,11] with antiferromagnetic interfacial coupling, in SRO/LSMO bilayer there is no

visible change in the shape of the hysteresis loops or the value of the exchange field upon field cycling for 4 times, owing to the frozen-in SRO spin structure.

Figure 2(d,e,f) shows simplified schematics illustrating the proposed depth profile of spin structures in both SRO and LSMO layers at low temperatures with different CFs. During the field-cooling process, the magnetic energy of SRO layer is the sum of the exchange energy ( $H_{ex}$ ), uniaxial anisotropy energy ( $H_K$ ), Zeeman energy ( $H_Z$ ), and the interfacial exchange energy ( $H_J$ ). Because of the large uniaxial anisotropy, the width of SRO domain wall is very narrow ( $\sim 3$  nm) [14] and the SRO spins projected in the plane can be approximated to be either parallel or antiparallel to the applied field; therefore, the SRO magnetic configuration is effectively determined by the competition of  $H_Z$  and  $H_J$ . Note that LSMO spins line up with the magnetic field at SRO transition during the cooling process with the CFs being much larger than LSMO coercive field. For a large CF,  $H_Z$  dominates over  $H_J$ , thus the SRO spins align parallel to LSMO layer (Fig. 2d), resulting in a single positively biased loop; for small CF,  $H_J$  is larger than  $H_Z$  such that the SRO moments prefer to be antiparallel to LSMO layer (Fig. 2f), leading to a single negatively biased loop; while for intermediate CF,  $H_Z$  and  $H_J$  are comparable to each other, forming lateral magnetic domains with opposite SRO spin orientations (Fig. 2e), which sequentially cause the double-loop shift of LSMO layer. Thus, the mechanism forming the double-loop hysteresis is different from what has been reported in other systems [15,16], which was either due to induced uniaxial anisotropy in the biased layer [15] or due to domains in the biased layer inducing a domain structure in the biasing layer [16]. According to Fig. 2(c), the net SRO moment is close to zero with 450 Oe CF, from which we can estimate the interfacial exchange energy  $H_J \sim H \cdot M_{SRO} \cdot t_{SRO}$  to be about  $0.11 \text{ erg/cm}^2$ , where  $M_{SRO}$  and  $t_{SRO}$  are the magnetization and thickness of the SRO layer respectively.

To confirm the spin structure discussed above and to obtain further insight on the magnetic and structural depth profile of the film we applied PNR technique [17,18] following the same cooling procedure previously described. The two-dimensional (2D) intensity maps of scattered neutrons were recorded to measure both specular and off-specular scattering. Figure 3(a, b, c) shows the reflectivity curves ( $R^+$  and  $R^-$ ) extracted from the 2D maps measured at 1000 Oe field after the sample was cooled down to 10 K in 1000 Oe, 100 Oe, and 500 Oe, respectively. The MSLD profiles of SRO and LSMO layers obtained from the fitting are plotted as functions of the distance from the surface, shown in Fig. 3(d). The magnetization of LSMO layer calculated from the obtained MSLD is about  $2.93 \mu_B/\text{Mn}$ , and the net in-plane magnetization of SRO layer is about ( $\pm$ )  $0.63 \mu_B/\text{Ru}$  and  $0.24 \mu_B/\text{Ru}$  for 1000 Oe (100 Oe) and 500 Oe CF respectively. These results are in a good agreement with values obtained from the SQUID data. The small net magnetization of the SRO layer for the 500 Oe CF supports a hypothesis about a formation of stripe lateral  $180^\circ$  magnetic domains with SRO spins oriented along the easy axis parallel or anti-parallel to the direction of CF and to the neutron polarization (see the inset of Fig.3(c)). In this geometry the net magnetization of SRO layer is determined as the mean value averaged over the stripe  $0^\circ$ - $180^\circ$  domains within the neutron coherence length and contributes to the specular reflectivity in the non spin-flip channel, while the deviation of magnetization from this mean value within each domain contributes to the off-specular scattering (also non spin-flip channel in this case). Figure 3(e) shows a 2D map of the reflected and scattered intensity for 500 Oe CF as a function of  $(p_i-p_f)$  and  $Q_z = (p_i+p_f)$  with  $p_{i(f)} = 2\pi\sin\theta_{i(f)} / \lambda$  the normal to the surface component and  $\theta_{i(f)}$  the angle of the incident (scattered) wave vector [19]. The specular scattering occurs at  $p_i = p_f$ . For the configuration shown in the cartoon in Fig. 3c the off-specular scattering appears as the Yoneda scattering [20] close to  $Q_c$  in the non spin-flip channel from stripe domains when the

$l_{Dx} < l_{cohx}$  (where  $l_{Dx}$  is domain size along the direction perpendicular to the neutron polarization direction and  $l_{cohx}$  is the lateral projection of the neutron coherence length) and is clearly seen in Fig. 3(e). Figure 3(f) shows the model calculation, which reproduces the details in Fig. 3(e). From the 2D model fit we obtained the width of the stripe domains of 200 nm, which is consistent with that observed in the bare SRO film by TEM [14].

To further prove the formation of in-plane stripe domains, we performed an additional experiment. After the sample was cooled down with 500 Oe CF, it was rotated by 90° at zero field around the axis normal to the film surface and then reflectivity measurement was done in a small magnetic guide field of 40 Oe field, which did not affect the magnetization in the film. In this geometry no off-specular scattering was recorded above the background, which suggests that in this direction the length of the stripe domains is larger than the lateral projection of the neutron coherence length  $l_{Dx} > l_{cohx}$ , as shown in the cartoon inserted in Figure 4. Since no off-specular scattering signal was observed, the spin-flip component contributes to the specular channel and was taken into account during the fit [21] as described in [18]. The moduli of the magnetization vectors in LSMO and SRO layers (obtained from the fit to the data for 1000 Oe CF) were kept fixed while the angles between the magnetization vectors for both LSMO and SRO layers and the direction of the neutron polarization were the only two parameters of the fit. Note that in this configuration the PNR reflectivity R+ (or R-) contains two spin-states,  $R^{++} + R^{+-}$  (or  $R^{--} + R^{-+}$ ) [21,22]. The overlapping  $R^{+}$  and  $R^{-}$  are indicative of a negligible magnetization component parallel to the neutron polarization. The angles of SRO and LSMO magnetic moments are determined to be close to 90°, i.e. perpendicular to the direction of the field and the neutron polarization (inset of Fig 4). This provides the direct evidence that the low temperature SRO moments were frozen-in and are aligned along the easy axis due to the strong uniaxial

anisotropy [12]. Further, due to coherence anisotropy in the reflectometry experiment [17,23] the domain size  $l_{Dx}$  should be larger than the lateral projection of the neutron coherence length [19]. This allows us to estimate the lower limit for the length of the stripe domains of 150-400 microns [23].

In summary, CF dependent spin structure of an epitaxial exchange-biased ferromagnetic oxide bilayer LSMO / SRO has been revealed by means of SQUID magnetometry and PNR measurements. The spin structure of the biasing SRO layer is determined by the balance of the Zeeman interaction and the interfacial coupling during the cooling process, which in turn affects the magnetization reversal process of the biased LSMO layer. The unexpected formation of lateral stripe magnetic domains within the biasing layer with the domain walls perpendicular to the interface leads to double-shifted hysteresis loops in the biased layer [24], the mechanism of which has not been reported in conventional exchange-bias systems.

The work was supported by the Scientific User Facilities Division, Office of Basic Energy Sciences, DOE and the National Science Foundation through grants ECCS-0708759 (C. B. E. and M.S. R.).

## FIGURE CAPTIONS

**Figure 1:** x-ray reciprocal space map about the (103) reciprocal lattice point showing the fully strained epitaxial SRO and LSMO layers grown on STO substrate. The diffraction peak spots from top to bottom correspond to LSMO, STO, and SRO, respectively. Bottom inset is a STM image showing the surface morphology and the top inset depicts the schematics of the bilayer structure.

**Figure 2:** (a) Temperature dependence of magnetic moment of the sample measured with a 1000 Oe field after the sample is cooled down with different CFs applied along the easy axis of SRO layer. The green dash-dotted curve shows the extracted LSMO magnetic moment. (b) Isothermal curves at  $T = 10$  K. (c) CF dependence of the SRO moment at 10 K extracted from the hysteresis loops. Inset shows the relationship between the SRO moment extracted from hysteresis loops and  $M(T)$  curves. Schematics (d,e,f) illustrate the depth profile of the in-plane projection of low temperature spin structure of the bilayer with large (d), intermediate (e), and small (f)  $H_{FC}$ . Note the lateral  $180^\circ$  magnetic domains of SRO layer in (e) with the domain wall width along the magnetic hard axis  $\sim 3$  nm [14] not shown.

**Figure 3:** Reflectivity data as a function of momentum transfer  $Q$  of the sample taken at 10 K in the external field of 1000 Oe after different CFs of 1000 Oe (a), 100 Oe (b), and 500 Oe (c), respectively. Symbols represent the experimental data and the solid curves are the fits described in the text. Inset show the sample setups (domain configurations) relative to the neutron polarization field  $H$ . The elliptic illustrates anisotropy of the neutron coherence length with  $l_{cohx} \gg l_{cohy}$ . The depth profiles of the magnetic scattering length density (MSLD) of the bilayer

extracted from the data fittings are shown in (d). The experimental (e) and calculated (f) two-dimensional maps of reflected and off-specular scattered intensity as functions of  $Q_z = (p_i - p_f)$  and  $(p_i + p_f)$ , respectively, with  $p_i$  and  $p_f$  being the components of the incident and scattered wavevectors perpendicular to the sample surface. The specular scattering occurs at  $p_i = p_f$ , while the off-specular scattering appears as the Yoneda scattering close to the  $Q_c$ . (The Yoneda off-specular intensity on the right-hand side in (e) was partially shaded by a mask on the detector).

**Figure 4:** Experimental reflectivity with the fit to the data as a function of momentum transfer  $Q_z$  of the sample, which was cooled down to 10 K with a 500 Oe field and then rotated by  $90^\circ$  at zero field. The top inset shows the depth profile of the angle between the magnetic moments of SRO and LSMO and the neutron polarization obtained from the fits to reflectivity curves. Both angles are close to  $90^\circ$ , i.e. perpendicular to the direction of the field and the neutron polarization. The bottom inset shows the sample setup with the domain configuration relative to the neutron polarization and the guide field  $H$ . The elliptic schematically illustrates anisotropy of the neutron coherence length with  $l_{\text{coh}x} \gg l_{\text{cohy}}$ .

- 
- <sup>1</sup> E. Dagotto, *Science* **318**, 1076 (2007).
- <sup>2</sup> See a review, J. Mannhart and D. G. Schlom, *Science* 327, 1607 (2010); and references therein.
- <sup>3</sup> X. Ke, M.S. Rzchowski, L.J. Belenky, and C.B. Eom, *Appl. Phys. Lett.* **84**, 5458 (2004)
- <sup>4</sup> M. Ziese, I. Vrejoiu, E. Pippel, P. Esquinazi, D. Hesse, C. Etz, J. Henk, A. Ernst, I. V. Maznichenko, W. Hergert, and I. Mertig, *Phys. Rev. Lett.* **104**, 167203 (2010).
- <sup>5</sup> See a review, J. Nogues and I.K Schuller, *J. Magn. Mag. Mat.* **192**, 203 (1999).
- <sup>6</sup> S. Mangin, G. Marchal, and B. Barbara, *Phys. Rev. Lett.* **82**, 4336 (1999).
- <sup>7</sup> M. Zhu, M. J. Wilson, B. L. Sheu, P. Mitra, P. Schiffer, and N. Samarth, *Appl. Phys. Lett.* **91**, 192503 (2007).
- <sup>8</sup> F.Y. Yang and C.L. Chien, *Phys. Rev. Lett.* **85**, 2597 (2000).
- <sup>9</sup> T. Hauet, J. A. Borchers, Ph. Mangin, Y. Henry, and S. Mangin, *Phys. Rev. Lett.* **96**, 067207 (2006).
- <sup>10</sup> J. Nogués, D. Lederman, T. J. Moran, and I. K. Schuller, *Phys. Rev. Lett.* **76**, 4624 (1996).
- <sup>11</sup> S. Mangin, F. Montaigne, and A. Schuhl, *Phys. Rev. B* **68**, 140404(R) (2003).
- <sup>12</sup> Q. Gan, R.A. Rao, C.B. Eom, L. Wu, and F. Tsui, *J. Appl. Phys.* **85**, 5297 (1999).
- <sup>13</sup> Y. Lee, B. Caes, and B. N. Harmon, *J. Alloys and Compounds* **450**, 1 (2008).
- <sup>14</sup> L. Klein, Y. Kats, A.F. Marshall, J.W. Reiner, T.H. Geballe, M.R. Beasley, A. Kapitulnik, *Phys. Rev. Lett.* **84**, 6090 (2000).
- <sup>15</sup> R.P. Michel, A. Chaiken, C.T. Wang, and L.E. Johnson, *Phys. Rev. B.* **58**, 8566 (1998); Chih-Huang Lai, Yung-Hung Wang, Ching-Ray Chang, Jyh-Shinn Yang, and Y.D Yao, *Phys. Rev. B.* **64**, 094420 (2001).

---

<sup>16</sup> N.J. Gökemeijer, J.W. Cai, and C.L. Chien, *Phys. Rev. B* **60**, 3033 (1999); Hong-Wu Zhao, W.N. Wang, Y.J. Wang, W.S. Zhang, and J.Q. Xiao, *J. Appl. Phys.* **91**, 6893 (2002).

<sup>17</sup> G. P. Felcher and A. Hoffmann, in *Handbook of Magnetism and Advanced Magnetic Materials*, Vol.3, ed. H. Kronmueller and S. P. S. Parkin (Wiley, New York, 2007), p.1211; H. Zabel, K. Theis-Broehl, B. P. Toperverg, in *Handbook of Magnetism and Advanced Magnetic Materials*, Vol.3, ed. H. Kronmueller and S. P. S. Parkin (Wiley, New York, 2007), p.1237.

<sup>18</sup> See Supplementary Materials for details.

<sup>19</sup> V. Lauter-Pasyuk, H. J. Lauter, B. P. Toperverg, L. Romashev, and V. Ustinov, *Phys. Rev. Lett.* **89**, 167203 (2002).

<sup>20</sup> Y. Yoneda, “Anomalous surface reflection of x rays,” *Phys. Rev.* **131**, 2010–2013 (1963).

<sup>21</sup> Fits were conducted using Spin-Flip-Without-Analysis program which takes into account both non-spin-flip and spin-flip components.

<sup>22</sup> S. J. Blundell, M. Gester, J. A. C. Bland, H. J. Lauter, V. V. Pasyuk, and A. V. Petrenko, *Phys. Rev. B* **51**, 9395 (R) (1995).

<sup>23</sup> V. Lauter-Pasyuk, *J. Phys. IV France* **1** (2007) page 4-6.

<sup>24</sup> We note that after our manuscript was submitted, a paper by Solignac et al [*Phys. Rev. Lett.* **109**, 027201 (2012)] was published where the authors reported an asymmetric hysteresis loop at a high CF and attributed this feature to the presence of domains in the LSMO layer with dual antiferromagnetic interfacial couplings. This is different from the single hysteresis loop we observed at high fields in this study, which might be related to the different sequences of the bilayers and the quality of the LSMO films due to the different growth temperatures.

Furthermore, the mechanism of the double hysteresis loops for intermediate CF that we

---

discussed in our study is fundamentally distinct from that of the asymmetric hysteresis loops reported by Solignac et al.

Figure 1.

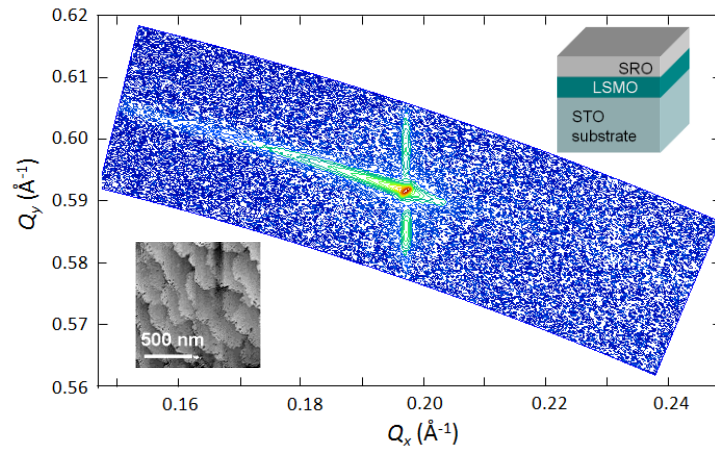


Figure 2.

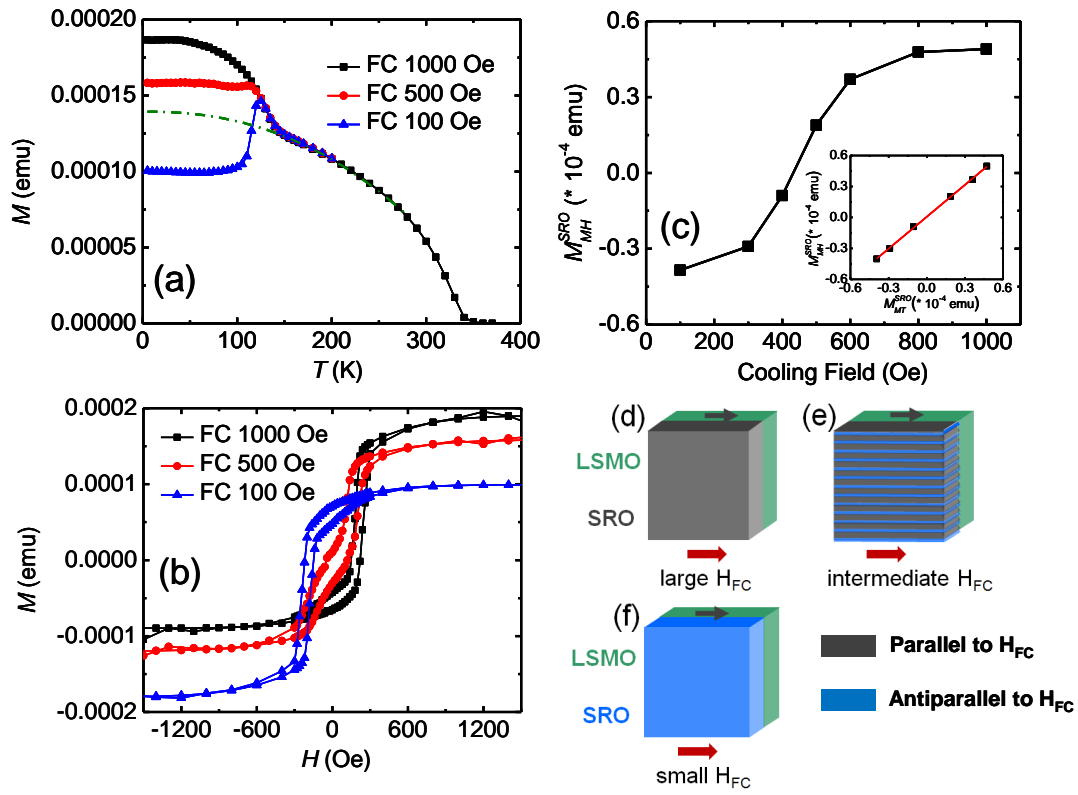


Figure 3.

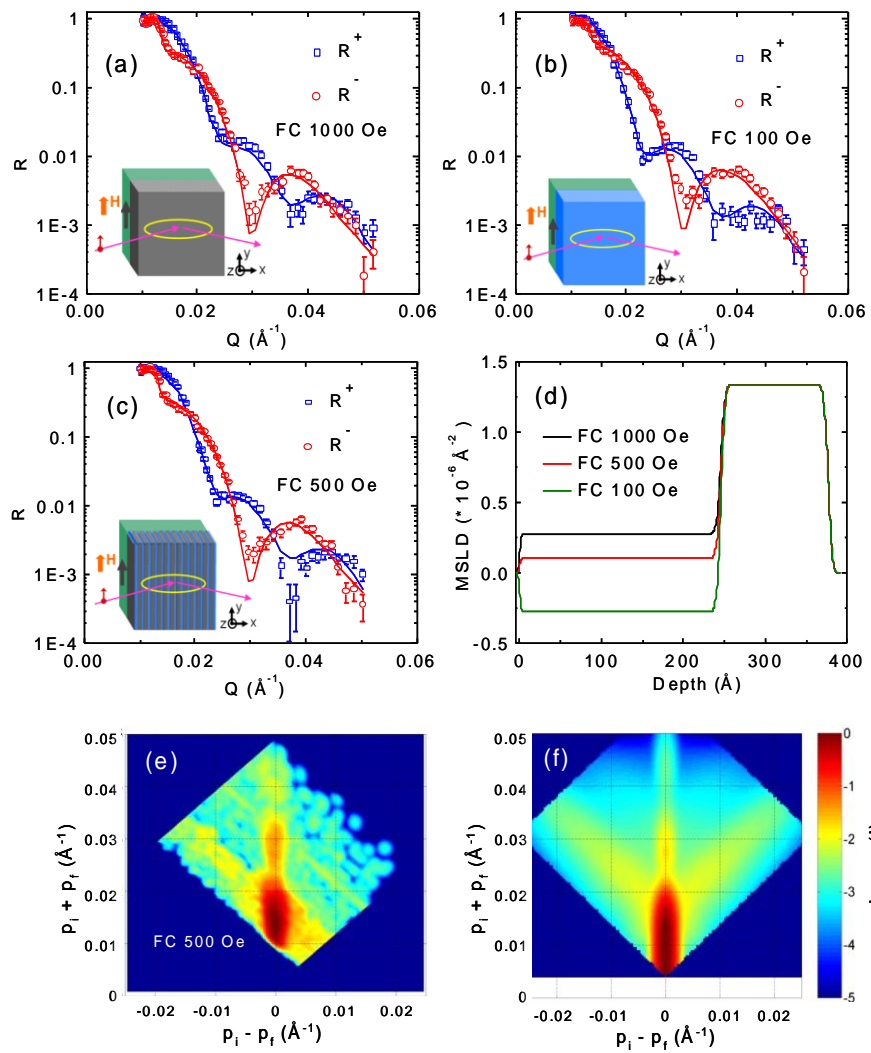


Figure 4.

